


Numerical simulation of carbonaceous raw material combustion in a coal seam channel

Vasyl Lozynskyi^{1*} 

¹ Dnipro University of Technology, Dnipro, Ukraine

*Corresponding author: e-mail lv.g.nmu@gmail.com

Abstract

Purpose. The research aims to investigate the combustion behavior of carbonaceous raw materials, specifically pulverized coal, in a cylindrical channel within a coal seam. The research focuses on understanding the temperature field dynamics, the distribution of combustion products, and the stabilization of the combustion process over time.

Methods. The research uses advanced Computational Fluid Dynamics (CFD) modeling using non-premixed combustion and the k-epsilon turbulence model. A cylindrical channel with a length of 30 m and a diameter of 1 m is selected, reflecting optimal conditions for co-gasification based on previous studies. Heat transfer processes are incorporated by activating the energy equation, accounting for heat generation from chemical reactions and its transfer via convection, conduction, and radiation. These considerations accurately represent the thermal and flow dynamics in the confined geometry.

Findings. The simulation indicates the temperature field stabilization, with a peak of 1540°C achieved in the combustion zone after 24 hours, gradually decreasing to approximately 520°C further downstream. Oxidation reactions are most active within the first 6 m of the channel, producing CO₂ as the primary combustion product. The flow velocity analysis indicates intense turbulence near the inlet, enabling efficient mixing of fuel and oxidizer. As the process progresses, turbulence intensity decreases, maintaining a steady distribution of thermal energy and stable downstream flow behavior.

Originality. The research has resulted in the development of a comprehensive methodology for modeling pulverized coal combustion process in geometrically constrained coal seam channels, representing the staged progression of the process (early, mid, and final stages). Patterns of temperature field stabilization and the distribution of chemical species along the channel have been identified.

Practical implications. The findings provide a foundation for optimizing underground coal combustion and co-gasification processes to improve geo-reactor systems' efficiency.

Keywords: coal, numerical simulation, temperature field, co-gasification, underground coal gasification

1. Introduction

Coal remains among the most abundant and widely used fossil fuels, critical in world energy production [1]. Despite the growing emphasis on renewable energy sources, coal remains valuable for industrial and energy sectors due to its high energy potential and widespread availability [2], [3]. However, conventional coal mining and utilization methods often have significant environmental challenges, including greenhouse gas emissions, surface degradation, and waste generation [4]-[7]. To address these issues, advanced thermal conversion methods, such as underground coal gasification (UCG), underground coal combustion (UCC), and co-gasification, have emerged as promising technologies for the efficient and sustainable utilization of coal reserves [8]-[12].

Underground coal gasification offers a unique approach by directly converting coal into syngas in situ, minimizing surface disturbance, and exploiting otherwise inaccessible reserves [13]-[16]. Similarly, underground coal combustion involves controlled burning of coal seams to extract energy while reducing

surface impacts [17]. Co-gasification, which combines coal with other carbonaceous materials such as biomass, further enhances the process by improving energy efficiency, reducing emissions, and expanding fuel flexibility [18]-[21]. These methods represent innovative approaches to maximize the utility of coal resources while addressing critical environmental and economic challenges, positioning them as essential technologies for the transition to cleaner energy solutions.

Thermochemical processes of coal conversion offer a potential way for developing deep or thin coal seams that are otherwise uneconomical using conventional mining techniques [22]-[25]. However, understanding the complex combustion dynamics in confined coal seam channels, including temperature profiles, species distributions, and flow behavior, remains challenging. Numerical simulation effectively solves these complexities, offering insights into optimizing operational parameters and improving overall efficiency [26]-[28]. It has become essential in optimizing and designing coal combustion systems, such as coal-fired power plants and industrial furnaces. Computational Fluid Dyna-

Received: 12 June 2024. Accepted: 5 December 2024. Available online: 30 December 2024

© 2024, V. Lozynskyi

Mining of Mineral Deposits. ISSN 2415-3443 (Online) | ISSN 2415-3435 (Print)

This is an Open Access article distributed under the terms of the Creative Commons Attribution License (<http://creativecommons.org/licenses/by/4.0/>), which permits unrestricted reuse, distribution, and reproduction in any medium, provided the original work is properly cited.

mics (CFD) models integrate sub-models for devolatilization, combustion, and heat transfer, allowing precise predictions of temperature distributions, gas concentrations, and flow patterns in combustion chambers [29]. Both Reynolds-Averaged Navier-Stokes (RANS) and Large-Eddy Simulation (LES) approaches have been widely adopted, with LES offering improved accuracy in determining turbulence effects in complex environments [30].

Open-source CFD codes like Code Saturne are utilized to diagnose inefficiencies in boiler operations, demonstrating their utility in identifying and mitigating operational bottlenecks [31]. However, CFD simulations often show discrepancies between numerical and experimental data in downstream regions of the combustor, where turbulence, heat transfer, and chemical interactions dominate [32]. These models are also instrumental in addressing environmental challenges, such as minimizing NO_x and SO_x emissions and solving operational issues like slagging and fouling in industrial furnaces [29].

Recent progress in high-fidelity simulations, including Direct Numerical Simulation (DNS) and LES, has significantly enhanced the understanding of pulverized coal combustion (PCC). DNS provides insights into particle-scale phenomena, revealing that smaller particles lead to upstream reaction zones with higher volatile matter concentrations, while higher mass loading correlates with increased heat release rates and temperatures [33]. LES simulations are also used to study large-scale furnace dynamics, highlighting the effects of turbulence on particle trajectories and heating rates [34].

The choice of devolatilization models is another critical factor in CFD accuracy. Models such as single-rate, two-competing rates, and chemical percolation devolatilization (CPD) significantly influence the prediction of volatile release and subsequent combustion reactions [35]. These advancements are particularly relevant for energy-intensive industries, such as cement production, where CFD is applied to enhance energy efficiency and reduce CO_2 emissions [36].

CFD techniques are extensively applied to specialized combustion systems, including rotary kilns and fluidized bed boilers. In rotary kilns, particle-scale heat transfer analysis revealed that convection accounts for up to 90% of heat transfer from kiln walls to coal particles, underscoring the importance of heat transfer dynamics [37]. Studies also show that reducing pellet size improves heat transfer and enables rapid reduction at lower temperatures [38].

The CFD simulations demonstrate core-annular flow structures in fluidized bed boilers and identify NO_x reduction strategies by optimizing primary air volume and coal particle size [39]. Comparative studies of coal combustion and gasification indicate higher production of H_2 and CH_4 during gasification, while CO levels depend heavily on oxygen availability [40]. These findings underscore CFD versatility in simulating complex systems to optimize operational efficiency.

Validation of experimental data remains critical for ensuring the accuracy of CFD models. CFD heat transfer and temperature gradient simulations in drop tube furnaces strongly agree with experimental data, particularly near the combustor inlet [41]. Similarly, Sakolaree et al. [42] validated CFD models of axisymmetric 2-D chambers, demonstrating reliable predictions for temperature distributions. Despite these successes, discrepancies often arise in down-

stream regions, where turbulence and chemical interactions become increasingly complex [32].

Recent advancements include applying novel methods like the Flamelet Generated Manifold (FGM), which models group combustion of coal particles. This approach reveals how higher particle densities increase ignition delays and alter flame shape [43]. Analytical counter-flow non-premixed combustion models demonstrate the effect of Stokes numbers on particle trajectories and highlight the heat loss impacts on overall system temperatures [44].

Additionally, ammonia/coal co-firing has emerged as a promising study area. Research shows that increasing ammonia ratios prolong ignition delays in low-oxygen environments, with homogeneous ignition dominating the process due to ammonia inhibitory effect on oxygen diffusion [45]. Similarly, Zhang et al. [46] developed a new burnout model incorporating pore volume correction, improving radiation prediction accuracy in coal-fired boilers.

Other studies have expanded the understanding of coal combustion dynamics through computational and experimental approaches. Ghose et al. [47] and Cai et al. [48] emphasized the importance of turbulence modeling, radiation effects, and devolatilization kinetics in improving the accuracy of CFD models for pulverized coal combustion. These studies highlighted how advanced CFD techniques can provide detailed insights into thermo-chemical phenomena, aiding the optimization of industrial furnaces. Miura [49] investigated coal combustion in blast furnace blowpipes, demonstrating the impact of turbulence and combustion models on predicting heat transfer and temperature gradients. Similarly, Chen et al. [50] used Direct Numerical Simulation (DNS) to analyze the influence of particle size, mass loading, and preferential concentration on reaction zones, revealing that smaller particles result in upstream combustion zones with enhanced heat release rates.

Zhang et al. [51] explored the coal char ignition kinetics, showing that ignition time increases with increasing particle size, but decreases with higher temperatures and pressures. Luu et al. [52] extended the study of particle combustion to iron particles in turbulent environments, revealing transitions from kinetic- to diffusion-limited oxidation with increasing temperatures. Barraza et al. [53] and Macphee et al. [54] focused on multiphase flow and heat transfer in rotary kilns, demonstrating the dominant role of convection in heat transfer to coal particles. These findings are further extended by studies on models incorporating eddy break-up (EBU) and kinetic parameter reactions, which provided valuable insights into fuel optimization and emission reductions [55]-[57].

The reviewed studies highlight the growing reliance on numerical methods to investigate coal combustion dynamics, optimize processes, and reduce emissions. Based on these advancements, this research focuses on the behavior of pulverized coal combustion in a cylindrical channel.

This research aims to better understand reaction zone evolution, temperature stabilization, and species distribution in confined geometries. By incorporating advanced turbulence models and heat transfer considerations, this research contributes to the broader goal of improving the efficiency and sustainability of coal combustion systems, serving as a foundational stage for the subsequent co-gasification process of coal seams and carbonaceous raw materials.

2. Materials and methods

2.1. Geometry

The computational domain is designed to replicate a typical gasification channel with a length of 30 m, based on prior calculations identifying this length as optimal for achieving effective gasification. The geometry consists of a cylindrical cavity formed within a coal seam, where pulverized coal is injected and combustion occurs.

To simulate the fuel and oxidizer supply, a concentric pipe-in-pipe configuration is implemented. The inner pipe (*fuel_inlet*) with a diameter of 10 cm injects pulverized coal, while the outer pipe (*air_inlet*) with a diameter of 20 cm delivers air as the oxidizer. This configuration ensures proper mixing of fuel and oxidizer within the channel.

At the opposite end of the channel, a circular outlet with a diameter of 20 cm allows the combustion products to exit the system. The inlet and outlet dimensions are selected to provide sufficient flow rates and maintain stable combustion conditions within the channel.

2.2. Mesh generation

The computational domain is discretized using a structured mesh to ensure high accuracy and stability in the simulation of combustion and flow dynamics (Fig. 1). The mesh is generated in with the following key parameters:

- the global element size is set to 1.0×10^{-3} m, ensuring a detailed geometry resolution;
- the minimum edge length is defined as 5.0×10^{-3} m, allowing for precise capture of flow gradients near boundaries;
- mesh curvature capture is enabled with a normal curvature angle, ensuring accurate representation of curved surfaces within the geometry.

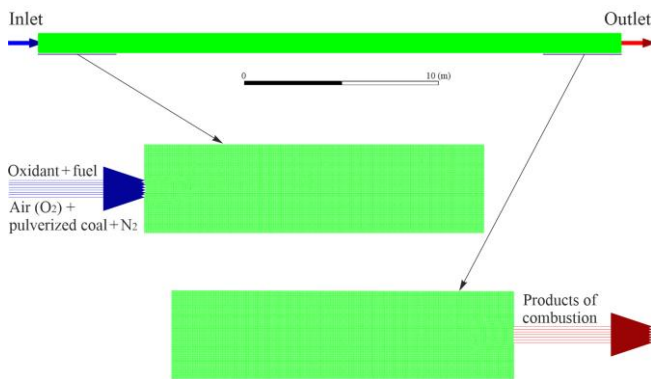


Figure 1. Schematic representation of the computational domain

The mesh comprises approximately 303066 nodes and 299965 elements, providing sufficient resolution for capturing flow and combustion phenomena. The diagonal length of the bounding box is 30.017 m, matching the physical length of the channel.

The mesh quality is validated to align with CFD best practices, ensuring reliable numerical performance throughout the simulation. Skewness is carefully controlled, maintaining values below 0.9, which is critical for minimizing numerical errors and ensuring solution accuracy. Additionally, medium smoothing is applied to further enhance the overall quality of the mesh elements, particularly in regions with complex flow dynamics.

Inflation layers with a smooth transition are implemented to accurately capture boundary layer effects near the channel walls and pipe inlets. The transition ratio is set to 0.272, with a maximum of two layers to provide gradual refinement from the walls to the core flow region. This approach ensures that the mesh can adequately resolve flow gradients and temperature profiles in critical zones.

2.3. Model parameters

2.3.1. Energy equation

The energy equation is enabled to model the transfer and distribution of heat generated by combustion reactions within the channel. This equation plays a crucial role in capturing temperature gradients, thermal expansion, and the effects of heat loss or gain due to conduction, convection, and radiation. The energy equation is expressed as:

$$\frac{\partial(\rho E)}{\partial t} + \nabla \cdot (\vec{v}(\rho E + p)) = \nabla \cdot \left(k_{eff} \nabla T - \sum_j h_j \vec{J}_j \right) + S_h, \quad (1)$$

where:

- ρ – the fluid density;
- E – the total energy per unit mass;
- \vec{v} – a velocity vector;
- k_{eff} – an effective thermal conductivity (includes effects of turbulence);
- T – a temperature;
- h_j – an enthalpy of species j ;
- S_h – volumetric heat source term (e.g., due to chemical reactions or radiation);
- \vec{J}_j – is the diffusion flux of species j .

The energy equation is essential for accurately predicting the thermal behavior in high-temperature combustion processes, such as pulverized coal combustion. It ensures that the effects of heat release from chemical reactions, thermal diffusion, and heat transport are taken into consideration. This is particularly critical for understanding the formation of high-temperature zones near the inlet and their evolution downstream.

2.3.2. Viscous model

The k-epsilon ($k-\epsilon$) turbulence model is selected due to its robustness and suitability for high Reynolds number flows, which are typical in combustion-driven systems. This model predicts the effects of turbulence on flow, mixing, and heat transfer by solving two transport equations: one for the turbulence kinetic energy (k) and another for its dissipation rate (ϵ). Turbulence kinetic energy (k) is calculated according to Equation (2):

$$\frac{\partial(\rho k)}{\partial t} + \nabla \cdot (\rho \vec{v} k) = \nabla \cdot \left(\frac{\mu_t}{\sigma_k} \nabla k \right) + G_k - \rho \epsilon, \quad (2)$$

where:

- μ_t – the turbulent viscosity;
- σ_k – the turbulent Prandtl number for k ;
- G_k – the turbulence kinetic energy production;
- $\rho \epsilon$ – a dissipation of k ;
- ∇ – is the nabla operator, which is used to denote spatial derivatives (it signifies the gradient, divergence, or Laplacian of a quantity depending on its context).

Turbulence dissipation rate (ε) is calculated according to Equation (3):

$$\frac{\partial(\rho\varepsilon)}{\partial t} + \nabla \cdot (\rho \vec{v} \varepsilon) = \nabla \cdot \left(\frac{\mu_t}{\sigma_\varepsilon} \nabla \varepsilon \right) + C_1 \frac{\varepsilon}{k} G_k - C_2 \rho \frac{\varepsilon^2}{k}, \quad (3)$$

where:

- σ_ε – the turbulent Prandtl number for ε ;
- C_1, C_2 – empirical constants.

Turbulent viscosity (μ_t) is calculated according to Equation (4):

$$\mu_t = \rho C_\mu \frac{k^2}{\varepsilon}, \quad (4)$$

where:

- C_μ – a model constant.

The k -epsilon turbulence model is selected for this research due to its suitability for high Reynolds number flows and ability to accurately capture turbulence characteristics in combustion-driven systems. The flow within the channel involves high-speed injection and intense mixing of fuel and oxidizer, making the k -epsilon model ideal for predicting the turbulence effects critical to non-premixed combustion processes. Additionally, this model balances accuracy and computational cost, providing reliable predictions for industrial-scale combustion systems while remaining computationally efficient. Its extensive validation in studies of high temperature reacting flows further underscores its robustness and reliability for modeling scenarios similar to those investigated in this work.

2.4. Combustion model

For this study, the non-premixed combustion model is chosen to simulate the combustion process within the cylindrical channel. This model is particularly well-suited for scenarios where the fuel and oxidizer are introduced separately and mix within the combustion zone, as is the case in the pipe-in-pipe configuration of the present system. The pulverized coal is injected through the central pipe, while air is supplied through the outer annular region, ensuring distinct fuel and oxidizer streams. This configuration creates a diffusion-dominated combustion regime, where the reaction rates depend primarily on mixing fuel and oxidizer.

The non-premixed combustion model is based on the mixture fraction approach, which simplifies the solution of chemical reactions by reducing the governing equations to a single scalar variable, the mixture fraction (f). This variable represents the local mass fraction of elements originating from the fuel stream. The combustion process is assumed to be in chemical or close to chemical equilibrium, allowing for the instantaneous reaction of the fuel and oxidizer when mixed. The key equation governing the mixture fraction is the transport Equation (5):

$$\frac{\partial(\rho f)}{\partial t} + \nabla \cdot (\rho \vec{v} f) = \nabla \cdot (\rho D \nabla f) + S_f, \quad (5)$$

where:

- ρ – the local gas density;
- f – the mixture fraction;
- \vec{v} – the velocity vector;
- D – the mass diffusivity;
- S_f – a source term accounting for contributions from fuel injection or chemical reactions.

The mixture fraction, denoted as f , is calculated using the Equation (6):

$$f = \frac{Z - Z_{ox}}{Z_{fuel} - Z_{ox}}, \quad (6)$$

where:

- Z – the carbon mass fraction in the mixture;
- Z_{ox} – the carbon mass fraction in the oxidizer;
- Z_{fuel} – the element mass fraction in the fuel.

This dimensionless quantity of f ranges from 0 (pure oxidizer) to 1 (pure fuel). It allows the determination of the local composition of the mixture, as well as predictions of temperature and concentrations of combustion products at each point in the flow. The mixture fraction allows for determining species concentrations and temperature through pre-computed equilibrium tables. This approach significantly reduces computational cost while maintaining accuracy in predicting combustion characteristics.

There are several reasons why this model is selected:

1. Pipe-in-pipe configuration inherently creates separate streams for the pulverized coal and air, making a diffusion-driven model ideal.
2. In pulverized coal combustion, mixing volatile species and oxygen primarily dictates the reaction rates, which the non-premixed model effectively captures.
3. The mixture fraction formulation simplifies the numerical solution, making it computationally efficient while accurately resolving the temperature and species profiles.

This model effectively captures the complex interactions between fuel and oxidizer, providing reliable predictions for temperature distribution, species concentrations, and overall combustion efficiency in the cylindrical channel.

2.5. Coal properties and particle settings

The coal properties are defined based on proximate and ultimate analyses (dry ash-free basis), which is essential for accurate combustion modeling. Both are calculated in weight percent (wt, %). Coal properties are summarized in Table 1.

Table 1. Ultimate and proximate coal analyses

Ultimate analysis (wt, %)				
C ^{daf}	H ^{daf}	O ^{daf}	N ^{daf}	S ^{daf}
80.7	6.3	6.8	4.9	1.3
Proximate analysis (wt, %)				
FC	V	A	M	
41.7	26.27	27.13	4.9	

The lower calorific value (LCV) of the coal, adjusted for dry ash-free (DAF) conditions, is computed using the formula presented in Equation (7):

$$LCV_{coal}^{daf} = \frac{HCV_{coal}^{ar} - h_{H_2O}^{latent} \cdot M - \frac{H_{ar} \cdot W_{H_2O}}{2 \cdot W_H} \cdot h_{H_2O}^{latent}}{1 - M - A}, \quad (7)$$

where:

- M and A – proximate analysis fractions for moisture and ash content, respectively;
- H_{ar} – the ultimate hydrogen fraction in the coal;
- W_{H_2O}, W_H – molecular weights of water and atomic hydrogen, respectively;
- $h_{H_2O}^{latent}$ – the latent heat of water.

Equation (7) accounts for the high calorific value (HCV) of coal on an as-received basis, corrected for moisture and ash content, as well as the latent heat of water vaporization. This formula ensures that coal effective calorific value is accurately determined, considering the thermodynamic losses due to moisture and ash. The computed LCV, along with the empirical fuel composition, serves as the foundation for defining the non-premixed combustion model and aligning the coal particle properties for accurate thermal and chemical simulation.

The coal particle material is defined as a “coal particle” with a high calorific value (HCV) of 2.46×10^7 J/kg, representing the coal energy content. Additional parameters include a high-temperature volatile yield of 1.0 and a fraction of nitrogen in char – 0.7. After inputting the coal properties, the following adjustments are automatically generated to align the model parameters with the defined fuel composition:

- an empirical fuel stream is created with a lower calorific value (LCV) of 3.46×10^7 J/kg;
- the non-adiabatic model is activated to account for heat losses, and the boundary species are set for inlet/outlet conditions;
- the material, called coal-particle, is defined with a volatile component fraction of 0.311 and a combustible fraction of 0.417, representing the volatile and fixed carbon contributions, respectively, in the combustion process;
- for accurate prediction of nitrogen oxide emissions, the volatile nitrogen mass fraction is set to 0.03803, and the char nitrogen mass fraction is set to 0.05590.

These parameters ensure precise modeling of combustion dynamics, volatile release, and NO_x formation, which are critical for understanding the thermal and chemical behavior of pulverized coal during non-premixed combustion.

2.6. Creation of the probability density function (PDF)

In non-premixed combustion modeling, the probability density function (PDF) method is widely employed to account for the effects of turbulence-chemistry interactions. The PDF approach describes the distribution of scalar quantities, such as temperature and species concentrations. Instead of solving for a single deterministic value, the method uses a statistical approach to represent fluctuations due to turbulence, particularly in mean mixture fraction (Z) and its variance. The mean mixture fraction is defined as the normalized mixing ratio of fuel and oxidizer:

$$Z = \frac{\text{Fuel Mass}}{\text{Fuel Mass} + \text{Oxidizer Mass}} \tag{8}$$

When $Z = 0$, the composition corresponds to pure oxidizer (e.g., air). When $Z = 1$, the composition corresponds to pure fuel. Intermediate values of Z represent zones where fuel and oxidizer are mixed to varying degrees, describing the transition between pure oxidizer and pure fuel regions.

The accuracy of the PDF-based combustion model in the non-premixed combustion approach is highly dependent on the correct specification of table parameters, which ensures an optimal balance between computational efficiency and solution accuracy. The grid point resolution is a critical parameter, where the initial number of grid points determines the starting resolution of the PDF table. In contrast, the maximum number of grid points sets an upper limit to refine the solution if necessary. This study sets values of 20 for the initial grid points and 200 for the maximum grid points,

which are typically sufficient to provide a well-resolved table without excessive computational cost.

The maximum change in value ratio and maximum change in slope ratio is set to 0.5, ensuring smoother gradients and refined convergence, particularly in regions with significant variations in species concentration or temperature. The maximum number of species in the table is set to 20, while the minimum temperature is defined as 25°C to maintain numerical stability and prevent unphysical results. Additionally, automated grid refinement is enabled to adaptively improve resolution in regions with sharp scalar gradients, ensuring accuracy without unnecessary computational overhead.

The graph of mean temperature as a function of the mean mixture fraction and scaled variance presented in Figure 2 is crucial for understanding the combustion process and validating the non-premixed combustion model. The PDF approach is used to describe the statistical behavior of temperature within regions where fuel and oxidizer mix.

The axes of the graph represent critical parameters for understanding the combustion process. The mean mixture fraction (Z) ranges from 0 to 1 (as described before).

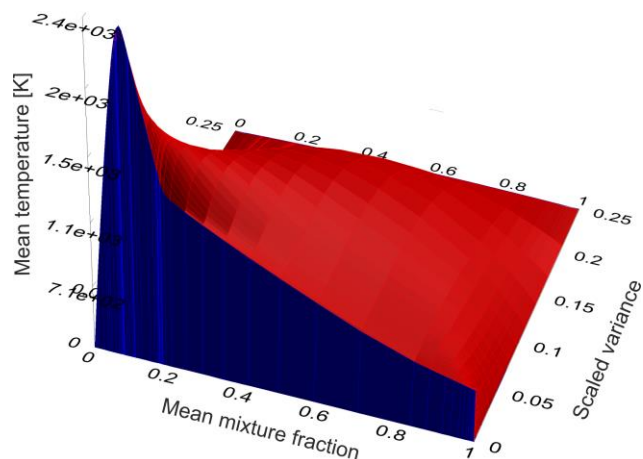


Figure 2. Mean temperature distribution as a function of mean mixture fraction and scaled variance for the non-premixed combustion model

The scaled variance accounts for fluctuations or turbulence in the mixing process, highlighting the variability in fuel-oxidizer interactions. The mean temperature (K) indicates the resulting temperature of the mixture under different mixing conditions, reflecting the energy release and combustion efficiency across the range of mixture fractions and turbulence intensities.

The highest temperature (more than 1500°C) is achieved at intermediate values of Z (around 0.04-0.19), where the optimal fuel-oxidizer ratio exists, and enabling complete combustion. At low mixture fractions, the temperature remains lower due to insufficient fuel for significant heat release. At high mixture fractions, temperature decreases because the lack of oxidizer limits combustion efficiency. The inclusion of scaled variance shows the impact of mixing fluctuations on temperature, which is essential for predicting localized hotspots or incomplete combustion zones.

So, this graph helps define the mean temperature distribution under varying fuel and oxidizer mixing conditions, providing essential input for subsequent simulations.

2.7. Boundary conditions

The air and fuel inlets are configured to ensure accurate representation of oxidizer and fuel supply, as well as turbulence effects at the boundaries. The air inlet is specified with a velocity value of 30 m/s, normal to the boundary, providing a consistent supply of oxidizer. Similarly, the fuel inlet is set with a velocity value of 7.7 m/s, also normal to the boundary, enabling pulverized coal injection. The turbulence intensity and viscosity ratio method is used in both inlets, with a turbulence intensity of 5% and a viscosity ratio of 10, reflecting moderate turbulence typical of confined channels. The air inlet is defined with a mean mixture fraction of 0 for species boundary conditions, indicating pure oxidizer. In contrast, the fuel inlet is set to a mean mixture fraction of 1, representing pure fuel. Both inlets include a mixture fraction variance of 0.125, accounting for boundary mixing fluctuations. These conditions ensure accurate mixing and combustion dynamics simulation at the inlet regions.

The outlet is specified as a pressure outlet with a zero-gauge pressure (approximately 0.101325 MPa under standard conditions), ensuring atmospheric pressure conditions. Back-flow conditions are modeled with a turbulence intensity of 5% and a viscosity ratio of 10 to account for potential recirculation or flow instabilities near the outlet. The mean mixture fraction and its variance are set to 0, indicating no additional species contributions or mixing from the outlet boundary.

2.8. Solution methods

The transient simulation uses the PISO scheme (Pressure-Implicit with Splitting of Operators) for pressure-velocity coupling, ensuring accurate resolution of unsteady dynamics associated with non-premixed combustion. The gradient is discretized using the Least Squares Cell-Based method, while pressure discretization uses the second-order scheme for enhanced accuracy. Momentum, energy, and mean mixture fraction equations are solved using the Second Order Upwind method to minimize numerical diffusion and improve solution accuracy. Turbulent kinetic energy and dissipation rate are discretized with the First Order Upwind scheme to balance computational efficiency and stability.

2.9. Transient simulation setup

In this research, the model is configured as a transient simulation to capture the temporal evolution of combustion dynamics at specific time intervals of 1, 12, and 24 hours. These intervals are selected to represent the early-stage, mid-stage, and near-final combustion behavior, providing critical insights into the progression and stabilization of key variables such as temperature, velocity, and species concentrations. The physical time intervals are converted into seconds (3600, 43200 and 86400 s) to ensure precise control over the simulation duration.

A small initial time-step size (e.g., 10^{-4} s) is used to achieve numerical accuracy and stability, adjusted on the Courant-Friedrichs-Lewy (CFL) condition. Adaptive time-stepping automatically adjusts the time-step size, allowing the solver to resolve fast physical processes like turbulent mixing and chemical reactions without compromising runtime efficiency. Data-saving intervals are defined using the "autosave" option in the calculation menu of activities, which ensures that results are saved specifically at 1, 12, and 24 hours, thus reducing storage requirements. Post-processing tools are then used to extract and analyze the results, including contour maps and plots for the selected time points.

3. Results and discussion

3.1. Temperature and specific heat distribution

The pulverized coal combustion within the cylindrical cavity is modeled to analyze the temperature and specific heat distributions along the channel at different time intervals (1, 12, and 24 hours). The results are presented in Figure 3 (contour maps) and Figure 4 (plots), highlighting the dynamic evolution of key parameters during the combustion process. Figure 4 provides a quantitative view of the parameters. The temperature and specific heat distributions evolve over time, but their overall patterns remain consistent.

The static temperature distribution (Fig. 3a and Fig. 4, top row) shows a distinct heating zone near the inlet, where the combustion process is most active. At 1 hour, the peak temperature reaches approximately 1220°C within the first 5 m of the channel. The temperature then sharply decreases and stabilizes around 520°C beyond 10 m. At 12 hours, the peak temperature rises to approximately 1490°C, and the high-temperature zone expands slightly further downstream, reflecting a more developed combustion process. By 24 hours, the maximum temperature increases to approximately 1540°C, with a similar spatial distribution, indicating that the combustion process reaches a relatively stable state.

A notable observation from the temperature profiles is temperature stabilization along the channel length in the downstream regions. Specifically, at 1 hour, the temperature between 5 and 30 m stabilizes at approximately 490-520°C, while for 12 and 24 hours, the temperature beyond 10 m shows a similar stabilization. This behaviour suggests that the combustion-generated heat is not effectively propagating downstream and is being rapidly dissipated.

Several factors can explain such stabilization. A significant portion of the heat could be lost through conduction into the surrounding coal seam, roof and bottom rocks. These materials typically have high thermal conductivity, facilitating heat transfer from the combustion zone. As a result, the downstream gas temperature does not increase significantly despite continued combustion upstream. Beyond the primary combustion zone (approximately the first 5-10 m), the availability of oxygen and volatile gases decreases, reducing heat release. The observed temperature range of 490-520°C may represent a state where the heat dissipation into the environment balances the heat generation from residual reactions. This quasi-steady-state behavior is typical in systems where energy losses to the environment are significant. Finally, while convective heat transfer plays a role in transporting energy along the channel, the dominance of conductive losses to the surrounding strata may limit the effectiveness of convective heat propagation. Radiative losses within the channel could also contribute but are generally less significant in this temperature range.

The observed temperature stabilization does not contradict the fundamental principles of thermal physics, but rather highlights the strong influence of conductive heat transfer in this system. In subsurface environments, the surrounding rock and coal layers act as significant heat sinks, effectively dispersing thermal energy away from the combustion zone.

The specific heat capacity distribution (Fig. 3b and Fig. 4, bottom row) closely correlates with the temperature profile, reflecting the changes in thermal energy along the channel length.

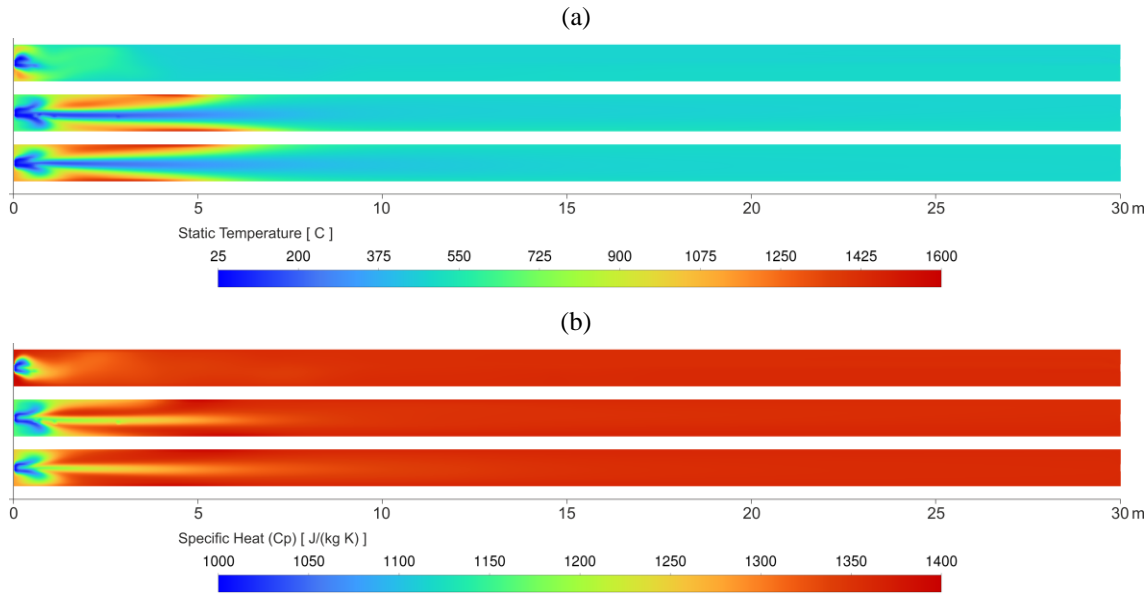


Figure 3. Contour maps of static temperature and specific heat distribution along the channel length at 1, 12, and 24 hours of pulverized coal combustion: (a) static temperature; (b) specific heat

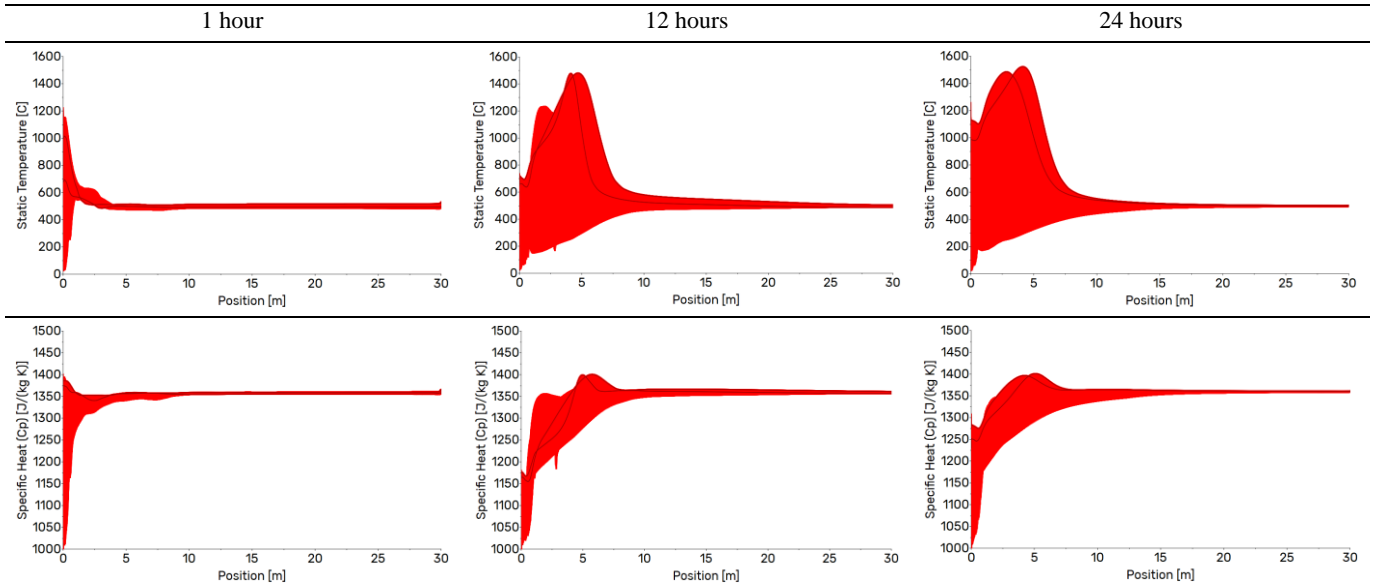


Figure 4. Plots of static temperature and specific heat distribution along the channel length at 1, 12, and 24 hours of pulverized coal combustion

The specific heat initially rises at the inlet region due to the high-temperature reactions. The peak specific heat values (approximately 1400-1500 J/kg·K) are observed close to the combustion zone for all time intervals. As the reaction products move downstream, the specific heat gradually decreases and stabilizes, similar to the temperature behavior.

The higher temperature observed near the channel walls compared to the center can be attributed to several factors. First, the turbulence flow near the walls enhances oxygen and pulverized coal mixing, leading to more intensive combustion reactions in these regions. The heat transfer dynamics also play a crucial role: conductive heat transfer from the hot gases to the surrounding coal seam and roof/bottom rocks may cause temporary heat accumulation near the walls. Furthermore, the slower flow velocity in the near-wall regions allows more heat to be retained locally, while the higher velocity in the center facilitates faster heat dissipation down-

stream. Radiative heat transfer and potential surface reactions on the channel walls may also contribute to localized heating. These phenomena collectively explain the observed temperature distribution and align with the thermophysical principles governing combustion and heat transfer in conditionally confined environments.

3.2. Non-combustible gaseous species

The distribution of non-combustible gaseous species, including oxygen (O₂), carbon dioxide (CO₂), and nitrogen (N₂), provides valuable insights into the combustion dynamics and efficiency along the channel length. Figures 5 and 6 illustrate spatial and temporal evolution of mass fractions at 1, 12, and 24 hours of pulverized coal combustion. These results enable a detailed assessment of oxygen consumption, the formation of carbon dioxide as a primary combustion product, and the role of nitrogen as an inert carrier gas during the process.

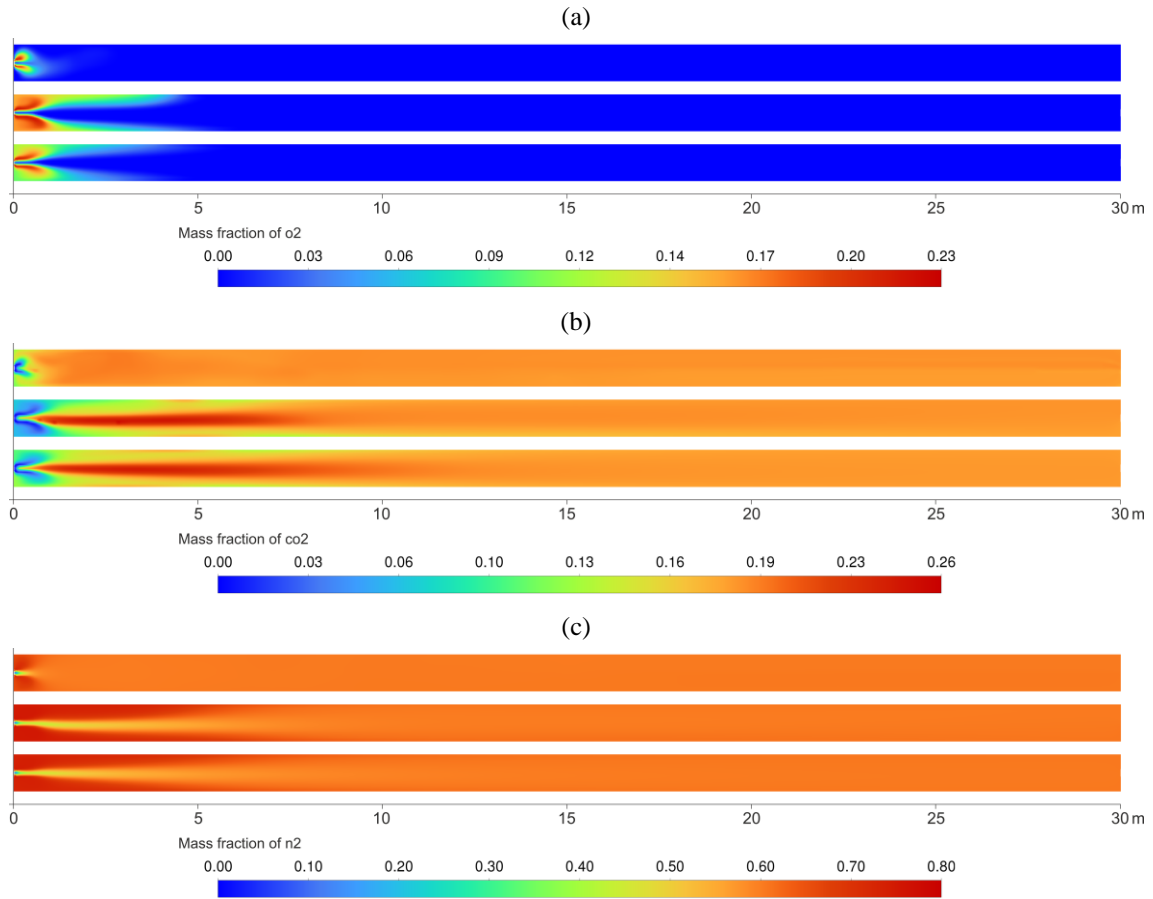


Figure 5. Mass fraction distribution maps of non-combustible gaseous species along the channel length at 1, 12, and 24 hours of pulverized coal combustion: (a) O_2 ; (b) CO_2 ; (c) N_2

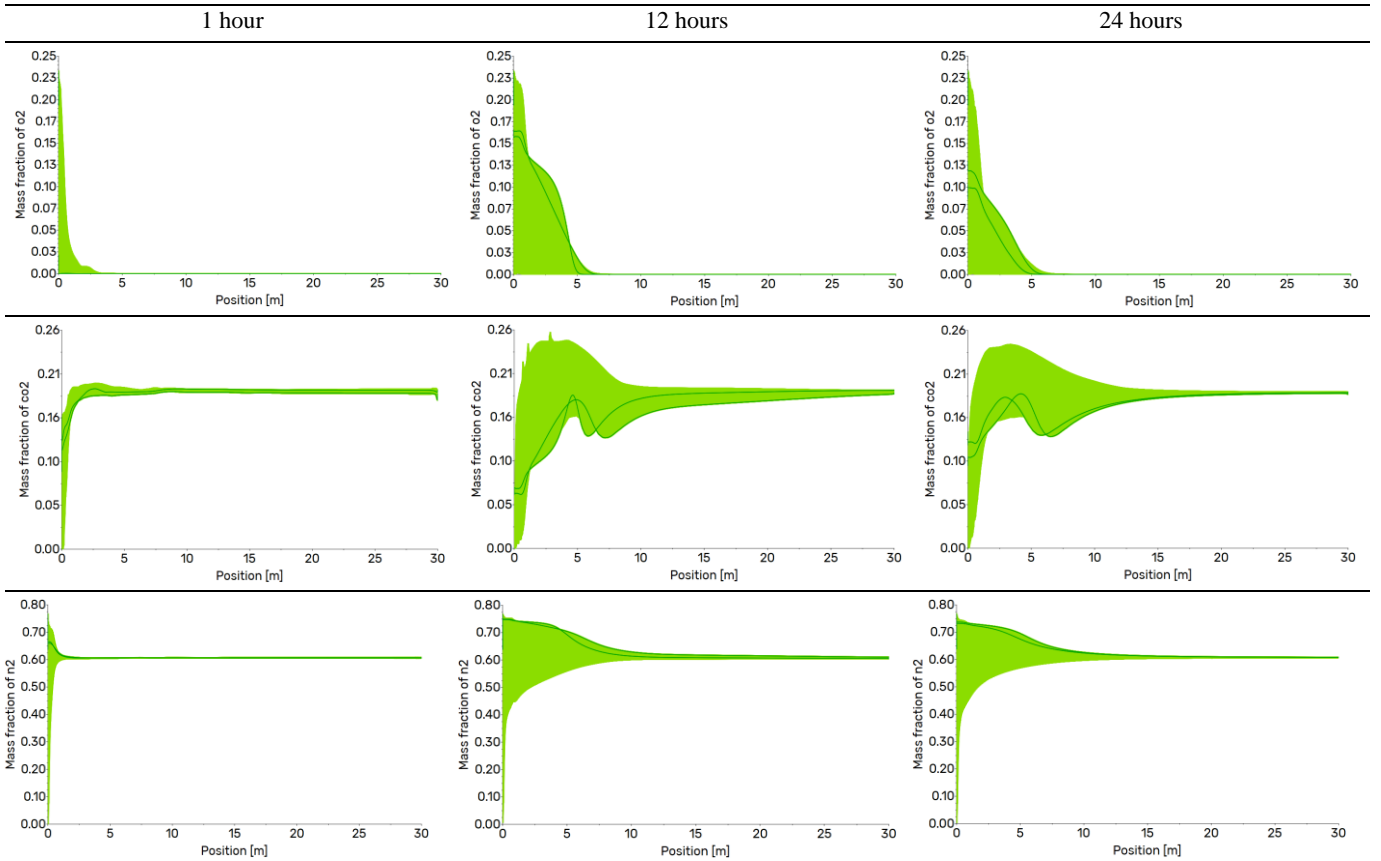


Figure 6. Plots of mass fraction distribution of non-combustible gaseous species (O_2 , CO_2 , N_2) along the channel length at 1, 12, and 24 hours of pulverized coal combustion

The mass fraction of oxygen (O_2) distribution decreases rapidly in the initial section of the channel at all time intervals (Fig. 5a). At 1 hour, oxygen reacts almost instantaneously, dropping its concentration to zero within the first 3 m of the channel. This indicates highly active combustion reactions near the inlet. Over time, at 12 hours, oxygen begins to diffuse downstream, with the depletion zone extending up to 6 m, reflecting the expansion of the combustion reaction zone. By 24 hours, a slight reduction in oxygen concentration is observed along the channel, but its distribution remains relatively stable beyond the primary combustion region. This stabilization suggests that the remaining oxygen cannot sustain significant downstream reactions, aligning with overall depletion of reactive gases in these regions.

The plots for oxygen (Fig. 6, top row) further illustrate this behavior, showing the sharp decline in mass fraction within the initial 3 m at 1 hour, which extends to 5-6 m at later time intervals.

Oxygen distribution along the channel contours rather than in the center is directly influenced by the injection configuration of fuel and oxidizer. Pulverized coal is injected through the central tube, concentrating the fuel in the channel core. At the same time, oxygen is supplied through the outer annular region, ensuring its initial concentration highest near the channel walls. This spatial separation creates a distinct reaction pattern: oxygen is consumed rapidly as it diffuses inward to the fuel-rich core, leading to near-zero concentrations in the center within the active combustion zone. Additionally, the higher turbulence near the fuel jet in the center enhances mixing and reaction rates, further accelerating oxygen depletion in the core. In contrast, the oxygen concentration remains higher near the walls due to slower diffusion and less direct interaction with the concentrated fuel stream. This configuration ensures efficient combustion near the inlet while limiting the oxygen availability downstream.

The mass fraction of carbon dioxide (CO_2) distribution exhibits a complementary trend to oxygen (Fig. 5b). CO_2 rapidly increases in the first 5-10 m, indicating that it is the primary combustion product of carbon-based fuels. In all time intervals, the highest concentration of CO_2 is observed near the inlet, where oxygen is actively reacting with pulverized coal. Beyond 10 m, the mass fraction of CO_2 stabilizes, reflecting the oxygen profile and suggesting limited further production downstream.

The CO_2 mass fraction trends shown in Figure 6 (middle row) highlight its complementary relationship with oxygen. At 1 hour, the CO_2 mass fraction rapidly increases within the first 5 m, peaking at approximately 0.20 and stabilizing downstream at around 0.18. By 12 and 24 hours, the CO_2 production zone shifts slightly downstream, as the combustion process evolves, with the peak mass fraction increasing to approximately 0.23-0.24 near the inlet. However, beyond 10 m, the CO_2 concentration remains stable at approximately 0.18, confirming that combustion reactions no longer occur in this region due to the depletion of oxygen and fuel. The fuel injection configuration directly influences the spatial distribution of CO_2 . Pulverized coal, supplied through the central tube, concentrates the combustion process near the channel center. As a result, the maximum CO_2 production is observed along the central axis of the channel, where fuel and oxygen interact most intensely. In contrast, the CO_2 concentration near the walls is relatively lower due to the

lower fuel concentration and limited combustion activity in these regions. This behavior highlights the strong dependence of CO_2 formation on the localized availability of fuel and oxygen within the combustion zone.

Nitrogen (N_2), an inert gas, shows a more uniform distribution along the channel (Fig. 5c). However, its concentration increases downstream, particularly in regions where oxygen and carbon dioxide stabilize. This behavior reflects the role of nitrogen as a carrier gas unaffected by chemical reactions and accumulating relatively smoothly as oxygen is depleted and combustion products dominate. Nitrogen, as an inert component, shows a stable mass fraction along the channel for all time intervals (Fig. 6, bottom row). Its relative concentration slightly increases downstream due to the depletion of reactive gases (O_2) and the accumulation of combustion products (CO_2). This behavior is consistent in all time intervals, with the mass fraction stabilizing at 0.6, highlighting the role of nitrogen as a passive ballast gas.

So, the initial 5-10 m of the channel represent the primary combustion zone, characterized by a rapid decrease in oxygen (O_2) and a simultaneous increase in carbon dioxide (CO_2). This behavior reflects the intense consumption of oxygen and its role in driving the combustion reactions that generate CO_2 as a significant product. The localized interaction of fuel and oxygen within this region highlights the high reactivity and energy release near the channel inlet. Beyond 10 m, the mass fractions of O_2 , CO_2 , and N_2 stabilize in all time intervals, indicating the completion of significant combustion reactions. The downstream region is predominantly influenced by the transport of inert gases or already-reacted combustion products. This stabilization is particularly evident for O_2 and CO_2 , where no further reaction occurs due to fuel and oxygen depletion in these zones.

Over time, the oxygen depletion and CO_2 production zones expand further downstream, as seen at 12 and 24 hours, reflecting the progressive spread of the combustion process and the stabilization of reaction zones as the system reaches equilibrium. The temporal shift highlights the adaptability of the combustion process and its dependency on the availability of reactive species. At 12 hours and 24 hours, the distributions of oxygen (O_2), carbon dioxide (CO_2), and nitrogen (N_2) are nearly identical. This similarity suggests that the system reaches a steady state within this time frame. The oxygen depletion and CO_2 production zones show minimal changes between these intervals, indicating that the combustion reactions and associated gas distribution have stabilized. The steady-state behavior reflects the equilibrium between the rates of oxygen supply, fuel consumption, and heat transfer within the system. This observation underscores the importance of the 12-24 hour range as a representative time interval for analyzing the stabilized performance of the combustion process.

3.3. Combustible gaseous species

The distribution of combustible gaseous species, including carbon monoxide (CO), methane (CH_4), and hydrogen (H_2), also provides valuable insights into the combustion dynamics and efficiency along the channel length. Figures 7 and 8 illustrate spatial and temporal evolution of mass fractions at 1, 12, and 24 hours of pulverized coal combustion. These results enable a detailed assessment of intermediate reaction products and their role in combustion.

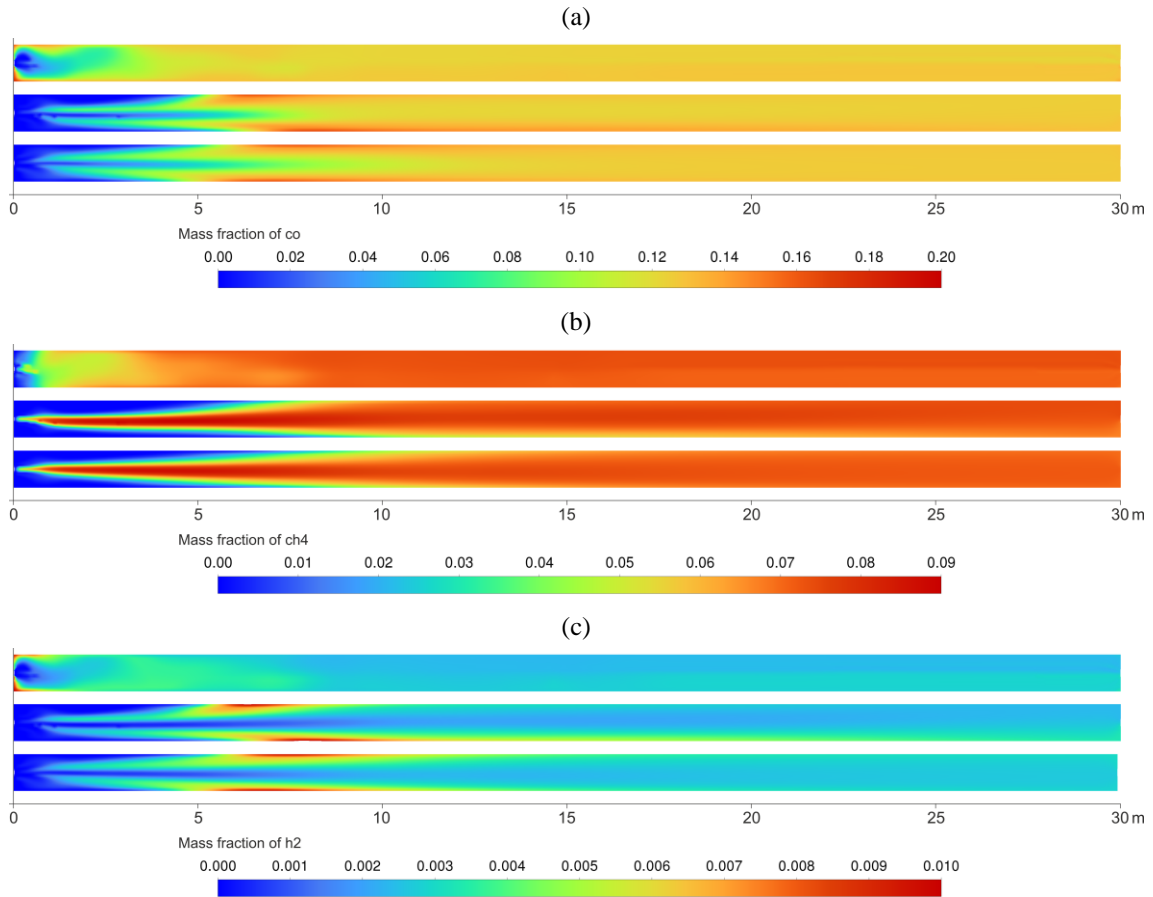


Figure 7. Mass fraction distribution maps of combustible gaseous species along the channel length at 1, 12, and 24 hours of pulverized coal combustion: (a) CO; (b) CH₄; (c) H₂

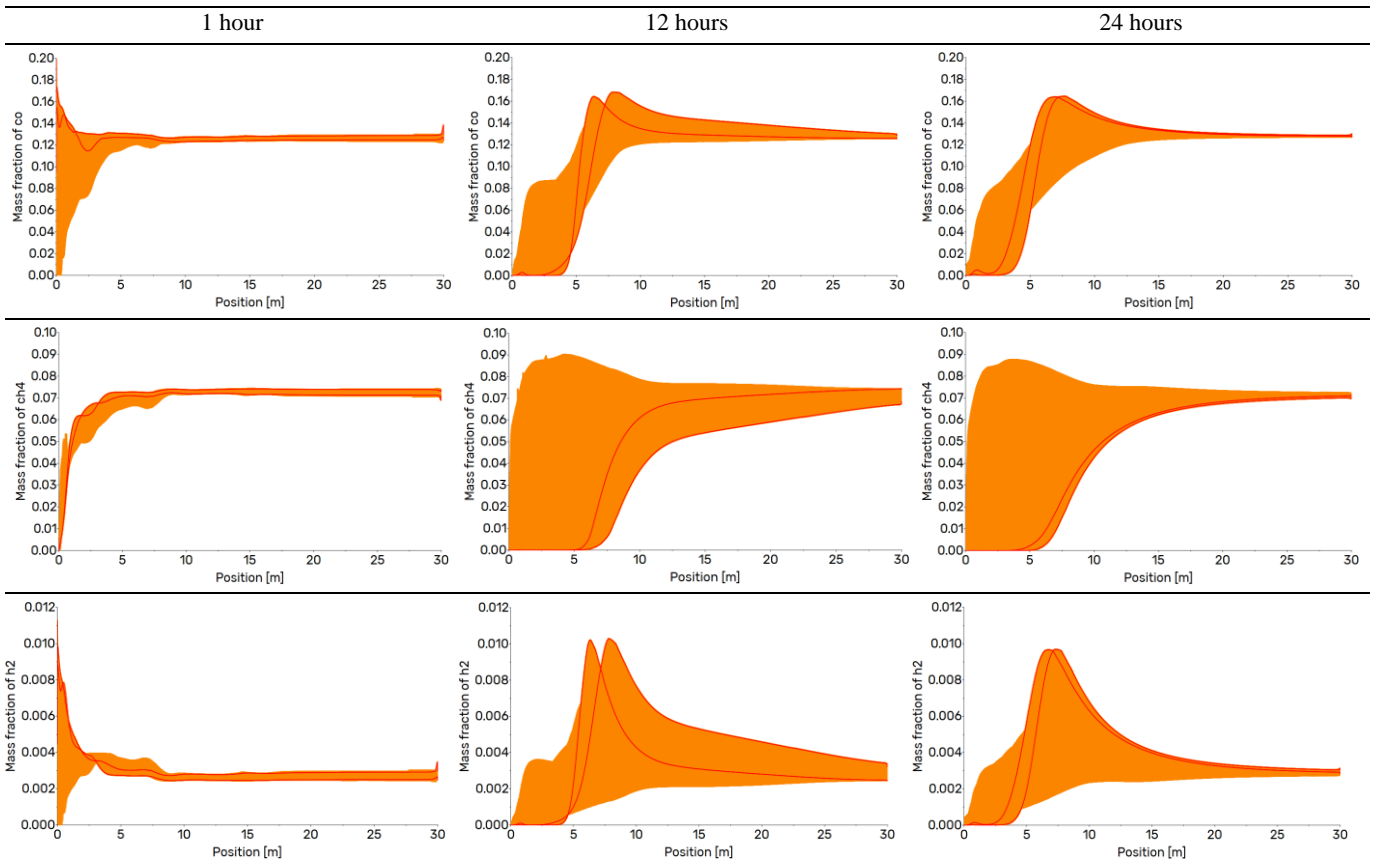


Figure 8. Plots of mass fraction distribution of combustible gaseous species (CO, CH₄, H₂) along the channel length at 1, 12, and 24 hours of pulverized coal combustion

The carbon monoxide (CO) mass fraction shows a distinct pattern along the channel length (Fig. 7a). At 1 hour, CO rapidly increases within the first 5 m. Peaking is reached at 12 hours, making approximately 0.17 at distances of 7-8 m. This behavior indicates incomplete combustion in the early stages, where oxygen is consumed, but not all intermediate products are fully oxidized. By 24 hours, the CO distribution becomes more uniform, with the same concentrations (around 0.13) in the middle and downstream regions, suggesting enhanced oxidation of CO to CO₂ as the combustion reactions stabilize over time. The plots for CO mass fraction (Fig. 8, top row) show a steep increase within the first 3-5 m at 1 hour, peaking at approximately 0.16-0.18 levels and then stabilizing at lower levels (~0.13) along the downstream region. At 12 and 24 hours, the CO production zone shifts slightly downstream, with higher concentrations extending to 6-10 m. However, the overall CO distribution remains stable beyond this point, suggesting that most of the CO has diffused downstream with minimal further reaction.

The methane (CH₄) mass fraction is concentrated near the inlet, peaking within the first 5-6 m at all time intervals, with a maximum value of approximately 0.06 (Fig. 7b). This indicates that methane is predominantly generated in the initial combustion zone as an intermediate product of coal pyrolysis. The CH₄ distribution exhibits its highest concentrations near the inlet, peaking at approximately 0.05 (Fig. 8, middle row). This peak shifts slightly downstream at 12 and 24 hours, reaching distances of 10 m, consistent with the progression of coal pyrolysis reactions. Beyond this zone, the methane mass fraction stabilizes at approximately 0.07, indicating that most of the CH₄ has been diffused downstream.

Hydrogen (H₂) exhibits a similar trend to CH₄, with its highest concentration near the inlet, peaking at 0.01 (Fig. 7c). The H₂ mass fraction decreases sharply downstream, stabilizing at negligible levels beyond 10 m. This behavior reflects the rapid consumption of hydrogen in oxidation and recombination reactions, particularly in the high-temperature combustion zone near the inlet. The distribution of H₂ (Fig. 8, bottom row) shows a sharp initial increase near the inlet, with maximum concentrations of approximately 0.01 at 1 hour, followed by a rapid decline beyond 5 m. At 12 and 24 hours, the H₂ production zone also shifts downstream, with peak values extending at 5-8 m. The H₂ concentration stabilizes in the downstream region at negligible levels (~0.003-0.0035), highlighting its quick consumption in high-temperature reactions and limited persistence further along the channel.

3.4. Combustible vs non-combustible gaseous species

The relationship between combustible and non-combustible gaseous species provides critical insights into the efficiency and progression of combustion reactions along the channel length. The combined analysis of key species such as oxygen (O₂), carbon dioxide (CO₂), carbon monoxide (CO), methane (CH₄), hydrogen (H₂), and nitrogen (N₂) offers a comprehensive view of the reaction dynamics, as illustrated in Figure 9.

Oxygen (O₂) undergoes rapid depletion within the first 3-5 m of the channel, aligning with the high-intensity combustion near the inlet. Simultaneously, carbon dioxide (CO₂), the primary combustion product, shows a complementary trend, rapidly increasing concentration and stabilizing downstream at approximately 18%. This stabilization reflects the near-complete conversion of oxygen and intermediate species into final combustion products in the upstream regions.

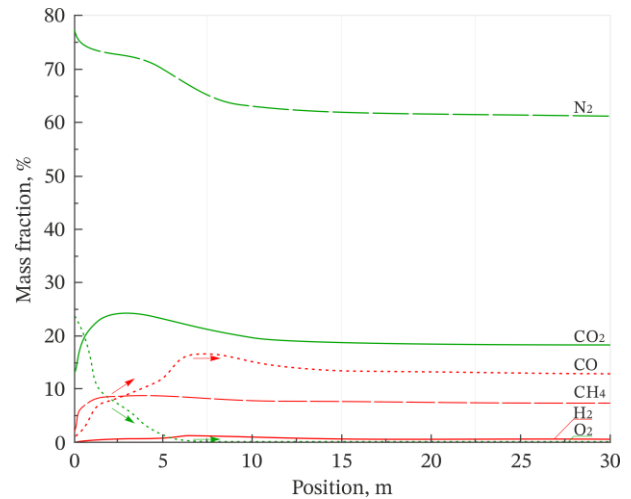


Figure 9. Combined mass fraction distribution of combustible (CO, CH₄, H₂) and non-combustible (O₂, CO₂, N₂) gaseous species along the channel length during pulverized coal combustion

Combustible intermediates, such as carbon monoxide (CO), methane (CH₄), and hydrogen (H₂), exhibit distinct patterns. CO peaks at the beginning of channel, suggesting its role as a transient species during incomplete combustion, and then gradually declining as it is oxidized to CO₂. Methane and hydrogen, both products of coal pyrolysis, are concentrated near the inlet and decrease sharply downstream due to rapid secondary reactions. The limited persistence of CH₄ and H₂ shows their efficient conversion into CO and CO₂ within the primary combustion zone. Nitrogen (N₂) remains unaffected by combustion, maintaining a stable concentration of approximately 62% in the second part of the channel. Its inert behavior reinforces its role as a diluting gas.

The interaction between combustible and non-combustible species illustrates the combustion process efficiency. The rapid consumption of O₂, the stabilization of CO₂, and the reduction of intermediates such as CO, CH₄, and H₂ demonstrate that the system effectively converts fuel into stable products, with minimal unburned species escaping downstream. These trends highlight the dominance of combustion reactions in the upstream regions and the eventual stabilization of gas compositions further along the channel.

Combustible gases such as CO, CH₄, and H₂ are formed during pulverized coal combustion primarily due to pyrolysis and incomplete oxidation reactions. During pyrolysis, high temperatures cause thermal coal decomposition, releasing volatile compounds that include methane and hydrogen. Simultaneously, insufficient oxygen in localized zones leads to partial oxidation of carbon, producing carbon monoxide as an intermediate species. These processes are inherent in complex reaction pathways during coal combustion.

3.5. Flow dynamics and their role in combustion

The study of flow parameters, including velocity value, turbulence intensity, and density, is crucial for understanding the physical processes that influence combustion efficiency and the distribution of gaseous species along the channel. Figures 10 and 11 illustrate spatial and temporal evolution of these parameters during pulverized coal combustion, providing insights into how the flow environment evolves and its impact on reaction zones and energy transfer.

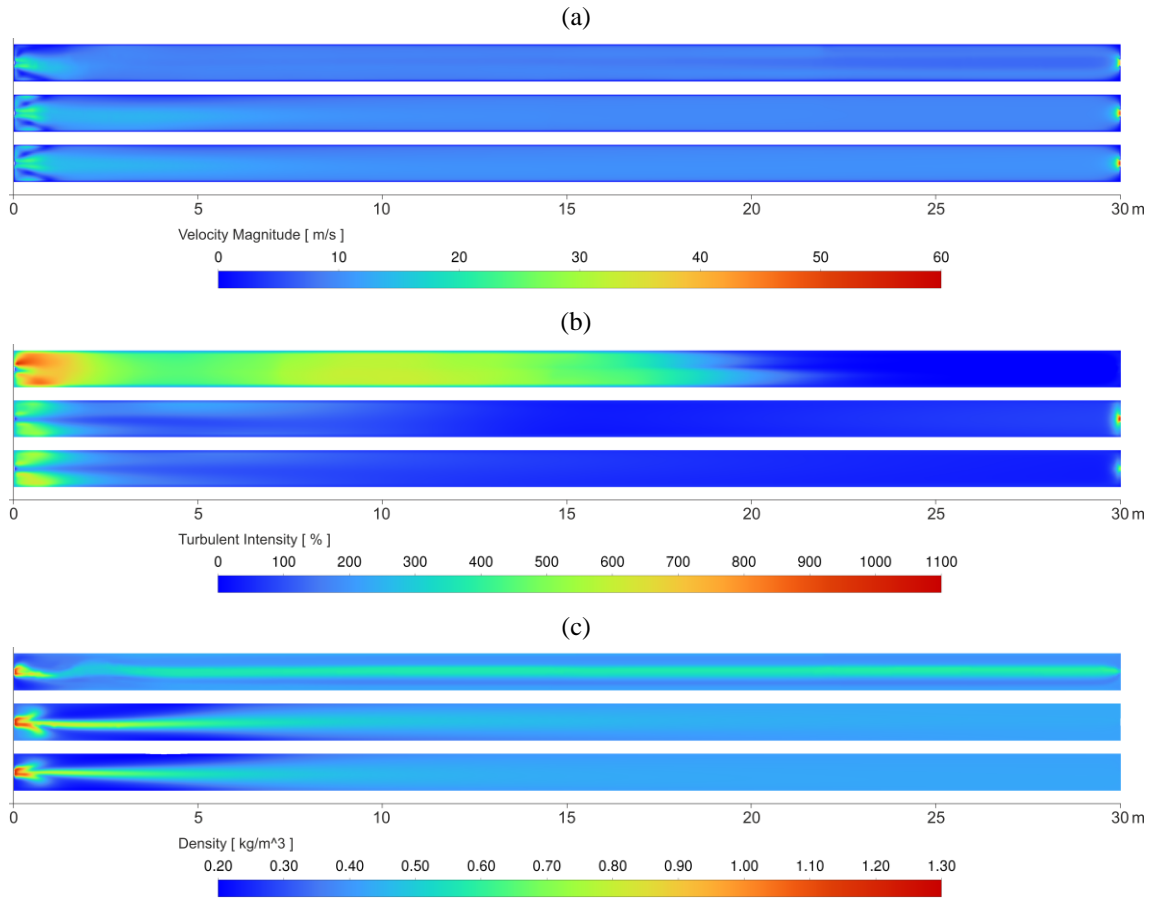


Figure 10. Distribution maps of flow parameters along the channel length at 1, 12, and 24 hours of pulverized coal combustion: (a) velocity value; (b) turbulence intensity; (c) density

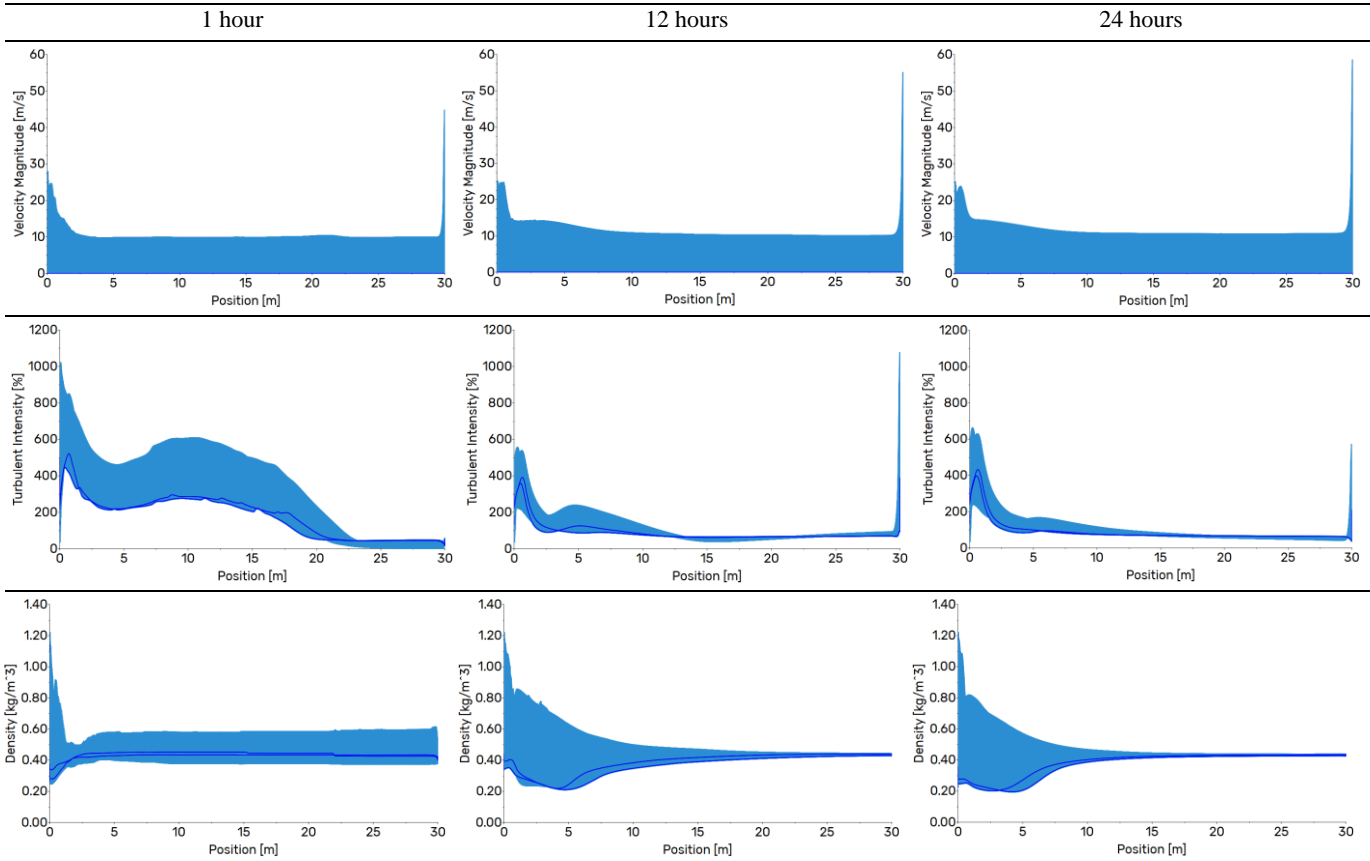


Figure 11. Plots of flow parameters distribution (velocity value, turbulence intensity, density) along the channel length at 1, 12, and 24 hours of pulverized coal combustion

Flow dynamics dictate the mixing of fuel and oxidizer, the transport of reactive species, and the removal of combustion products, thereby playing a critical role in the progress and stability of the combustion process.

The velocity value (Fig. 11, top row) along the channel demonstrates a distinct profile, with the highest values near the inlet and outlet, which is related to the geometric dimensions of the inlet and outlet. Throughout the entire combustion process of pulverized coal, the velocity at the inlet remains approximately 25 m/s, reflecting the initial dynamics of the pulverized coal and air mixture injection. As the flow progresses downstream, the velocity decreases and stabilizes at around 10-15 m/s, indicating a more uniform flow regime. The velocity profiles remain unchanged over 24 hours, indicating a steady-state flow condition with minimal variations along the channel.

As combustion progresses, the gas mixture temperature increases significantly, leading to thermal expansion. The combustion zone stabilizes over time, and a greater volume of gases expands, generating higher pressure within the channel. This increased pressure drives a higher flow velocity at the outlet. Also, combustion produces lighter gaseous species (e.g., CO₂, H₂O) and high-temperature gases with lower density. According to the continuity equation ($\rho v A = \text{const}$), the decrease in gas density (ρ) is compensated by an increase in velocity (v) at the outlet. Finally, efficient combustion enhances the thermal expansion of gases, increasing their velocity as they exit, which explains the high-velocity rate (up to 58 m/s) on the outlet side of the chamber.

The turbulence intensity exhibits its maximum values near the inlet, exceeding 800-1000% due to the high-speed injection and intense mixing of fuel and oxidizer (Fig. 11, middle row). At 1 hour, turbulence decreases gradually along the channel, stabilizing at lower levels (~200-300%) beyond 10 m. At 12 and 24 hours, the turbulence intensity follows a similar trend, but shows slightly reduced peaks near the inlet, indicating a more stable mixing regime as the combustion process evolves. The downstream stabilization of turbulence intensity supports efficient energy transfer and gas mixing in this region.

The turbulence intensity exhibits its maximum values near the inlet, exceeding 800-1000% due to the high-speed injection and intense mixing of fuel and oxidizer at 1st hour (Fig. 11, middle row). Then, along the channel, the turbulence decreases gradually, stabilizing at lower levels (~250-600%). The final 7 m demonstrate a low level of turbulence intensity. At 12 and 24 hours, the turbulence intensity follows a similar trend, but shows slightly reduced peaks near the inlet, indicating a more stable mixing regime as the combustion process evolves. The downstream stabilization of turbulence intensity supports efficient energy transfer and gas mixing in this region.

The density profiles highlight the dynamic changes in gas properties along the channel (Fig. 11, bottom row). Near the inlet, the density peaks are about 1.3 kg/m³, which correspond to the cold air-fuel mixture entering the channel. As the combustion reactions proceed, density decreases sharply due to the high temperatures and the production of lighter gaseous species. Beyond 10 m, the density stabilizes at approximately 0.4-0.6 kg/m³, reflecting the fully combusted gas mixture and its transport to the outlet. At 12 and 24 hours, the density profiles remain consistent, confirming the establishment of a steady-state combustion environment.

So, it is essential to summarize that the highest velocity value near the inlet and outlet highlight the impact of injection and exhaust processes on the overall flow regime. High turbulence near the inlet promotes effective mixing of the fuel and oxidizer, which is critical for initiating combustion. The downstream reduction in turbulence reflects the stabilization of flow conditions, and the sharp decrease in density near the combustion zone indicates the effect of high temperatures and gas expansion during combustion. Finally, the stable density downstream indicates complete combustion and gas transport efficiency.

3.6. Prospects for future research

The current study provides a detailed investigation of the temperature stabilization, reaction zone evolution, and species distribution within a confined channel during pulverized coal combustion. However, several avenues for future research remain to enhance the understanding of combustion dynamics and improve the practical application of these findings.

One promising direction involves the study of heat propagation into the surrounding roof and bottom strata of the coal seam. This would provide parameters for the thermal effects on the geological structure surrounding the combustion channel and help evaluate the risks associated with subsidence and changes in the mechanical properties of the rock mass and coal seam in the direction of the gasification panel.

Another critical area for exploration is the influence of external physical fields, such as magnetic or electric fields, on energy activation. Modifying activation energy could affect reaction rates and temperature distribution, offering new possibilities for optimizing combustion processes and increasing efficiency in specific conditions.

Additionally, future research should focus on the impact of varying carbonaceous fuel compositions, including biomass and coal particle mixtures, on temperature fields and combustion dynamics. Understanding how different fuels alter heat transfer, reaction zones, and emission characteristics will aid in developing sustainable co-gasification processes and expanding the applicability of underground coal combustion technologies. These studies, integrating advanced simulation methods and experimental validation, will help further refine predictive models and optimize combustion and co-gasification processes for energy efficiency.

4. Conclusions

This research provides a detailed numerical analysis of pulverized coal combustion within a confined cylindrical channel, addressing critical aspects of reaction zone dynamics, temperature stabilization, and species distribution. Using advanced computational models, incorporating turbulence and heat transfer mechanisms, it advances the understanding of non-premixed combustion.

An integrated methodology combining advanced turbulence modeling (k-epsilon) and non-premixed combustion frameworks has been developed to simulate pulverized coal combustion in a cylindrical channel. This approach enables precise characterization of reaction zones and thermophysical properties, which is necessary for understanding underground coal combustion dynamics.

Distinct stabilization of temperature profiles along the channel is observed, with a peak temperature of 1540°C achieved after 24 hours near the combustion zone. Downstream, the temperature stabilizes at approximately 520°C,

due to significant heat dissipation into the surrounding strata. Temperature temporal and spatial behavior highlights critical zones for reaction efficiency, emphasizing the impact of confined geometries on thermal propagation.

The research indicates a progressive evolution of combustion behavior, transitioning through early-stage, mid-stage, and near-final combustion phases. During the early stage, rapid oxygen consumption and steep temperature gradients are observed near the inlet, marking intense reaction activity. The mid-stage demonstrates an expansion of reaction zones downstream, with more uniform temperature distributions and improved mixing efficiency. By the near-final stage, the combustion system stabilizes, achieving steady-state conditions characterized by consistent temperature profiles and species distributions. This staged progression underscores the dynamic nature of combustion processes and the importance of stabilization for efficient energy transfer.

Novel insights into the interaction between oxygen depletion, CO₂ formation, and the distribution of intermediate species such as CO and CH₄ have been obtained. Rapid oxygen consumption within the first 6 m underscores the efficiency of the combustion process in upstream regions. At the same time, the stabilization of species concentrations downstream reflects the transition to steady-state conditions. Also, an analysis of velocity and turbulence intensity confirms the importance of flow-driven mixing in sustaining combustion. High turbulence near the inlet facilitates effective fuel-oxidizer interaction, while the gradual stabilization of flow parameters downstream ensures steady energy transport and species distribution.

This research demonstrates the potential for optimizing underground coal combustion systems by fine-tuning inlet parameters, fuel compositions, and channel geometries. It lays the groundwork for future advances in hybrid co-gasification processes, highlighting the importance of integrating coal-biomass combustion for sustainable energy generation.

A basis for further exploration of advanced combustion phenomena has been created. Future research should consider thermal interactions with geological formations, the influence of external physical fields on activation energy, and the impact of varying fuel compositions, including biomass.

Funding

The presented results have been obtained within the framework of the research works GP-512 “Co-gasification of carbon-containing raw materials during ultrathin coal seams gasification with a focus on hydrogen production”, state registration No. 0123U100985 and GP-511 “Scientific and practical foundation of structural transformations of coal-mining enterprises based on innovative technologies for rational environmental management” funded by the Ministry of Education and Science of Ukraine.

Acknowledgements

The author expresses gratitude to the heading editor and anonymous reviewers for valuable suggestions and recommendations taken into consideration during revision.

Conflicts of interests

Author VL declared that he was Deputy Editor in Chief of the *Mining of Mineral Deposit* journal at the time of submission. This had no impact on the peer review process and the final decision.

Data availability statement

The original contributions presented in the study are included in the article, further inquiries can be directed to the corresponding author.

References

- [1] Singh, V. (2024). Energy resources. *Textbook of Environment and Ecology*, 185-206. https://doi.org/10.1007/978-981-99-8846-4_12
- [2] Magdziarczyk, M., Chmiela, A., Dychkovskiy, R., & Smoliński, A. (2024). The cost reduction analysis of green hydrogen production from coal mine underground water for circular economy. *Energies*, 17(10), 2289. <https://doi.org/10.3390/en17102289>
- [3] Bondarenko, V., Griadushchiy, Y., Dychkovskiy, R., Korz, P., & Koval, O. (2007). Advanced experience and direction of mining of thin coal seams in Ukraine. *Technical, Technological and Economical Aspects of Thin-Seams Coal Mining, International Mining Forum, 2007*, 2-7. <https://doi.org/10.1201/noe0415436700.ch1>
- [4] Azadi, M., Northey, S.A., Ali, S.H., & Edraki, M. (2020). Transparency on greenhouse gas emissions from mining to enable climate change mitigation. *Nature Geoscience*, 13(2), 100-104. <https://doi.org/10.1038/s41561-020-0531-3>
- [5] Petlovanyi, M., Sai, K., Malashkevych, D., Popovych, V., & Khorolskiy, A. (2023). Influence of waste rock dump placement on the geomechanical state of underground mine workings. *IOP Conference Series: Earth and Environmental Science*, 1156(1), 012007. <https://doi.org/10.1088/1755-1315/1156/1/012007>
- [6] Pivnyak, G., Bondarenko, V., Kovalevs'ka, I., & Iliashov, M. (2013). *Mining of mineral deposits*. London, United Kingdom: CRC Press, 372 p. <https://doi.org/10.1201/b16354>
- [7] Petlovanyi, M., Medianyuk, V., Sai, K., Malashkevych, D., & Popovych, V. (2021). Geomechanical substantiation of the parameters for coal auger mining in the protecting pillars of mine workings during thin seams development. *ARPN Journal of Engineering and Applied Sciences*, 16(15), 1572-1582.
- [8] Bazaluk, O., Lozynskiy, V., Falshtynskiy, V., Saik, P., Dychkovskiy, R., & Cabana, E. (2021). Experimental studies of the effect of design and technological solutions on the intensification of an underground coal gasification process. *Energies*, 14(14), 4369. <https://doi.org/10.3390/en14144369>
- [9] Blinderman, M.S., & Klimenko, A.Y. (2017). *Underground coal gasification and combustion*. Amsterdam, the Netherlands: Woodhead Publishing, Elsevier, 650 p. <https://doi.org/10.1016/C2014-0-03452-1>
- [10] Li, R., Yang, Z., & Duan, Y. (2023). Energy, economic and environmental performance evaluation of co-gasification of coal and biomass negative-carbon emission system. *Applied Thermal Engineering*, 231, 120917. <https://doi.org/10.1016/j.applthermaleng.2023.120917>
- [11] Dychkovskiy, R., Dyczko, A., & Šošćarić, S.B. (2024). Foreword: Physical and chemical geotechnologies-innovations in mining and energy. *E3S Web of Conferences*, 567, 00001. <https://doi.org/10.1051/e3sconf/202456700001>
- [12] Mallick, D., Mahanta, P., & Moholkar, V.S. (2017). Co-gasification of coal and biomass blends: Chemistry and engineering. *Fuel*, 204, 106-128. <https://doi.org/10.1016/j.fuel.2017.05.006>
- [13] Dychkovskiy, R., Shavarskiy, J., Cabana, E.C., & Smoliński, A. (2019). Characteristic of possible obtained products during the well underground coal gasification. *Solid State Phenomena*, 291, 52-62. <https://doi.org/10.4028/www.scientific.net/SSP.291.52>
- [14] Kačur, J., Laciak, M., Durdán, M., & Flegner, P. (2023). Investigation of underground coal gasification in laboratory conditions: A review of recent research. *Energies*, 16(17), 6250. <https://doi.org/10.3390/en16176250>
- [15] Lavis, S., & Mostade, M. (2023). Underground coal gasification. *The Coal Handbook*, 323-337. <https://doi.org/10.1016/B978-0-12-824328-2.00010-8>
- [16] Bondarenko, V.I., Falshtynskiy, V.S., & Dychkovskiy, R.O. (2009). Synthetic stowing of rockmass at borehole underground coal gasification (BUCG). *Deep Mining Challenges: International Mining Forum 2009*, 169-177. <https://doi.org/10.1201/noe0415804288.ch18>
- [17] Blinderman, M.S., & Klimenko, A.Y. (2018). Introduction to underground coal gasification and combustion. *Underground Coal Gasification and Combustion*, 1-8. <https://doi.org/10.1016/B978-0-08-100313-8.00001-3>
- [18] Wei, J., Wang, M., Wang, F., Song, X., Yu, G., Liu, Y., Vuthaluru, H., Xu, J., Xu, Y., Zhang, H., & Zhang, S. (2021). A review on reactivity characteristics and synergy behavior of biomass and coal co-gasification. *International Journal of Hydrogen Energy*, 46(33), 17116-17132. <https://doi.org/10.1016/j.ijhydene.2021.02.162>

- [19] Wang, M., Wan, Y., Guo, Q., Bai, Y., Yu, G., Liu, Y., Zhang, H., Zhang, S., & Wei, J. (2021). Brief review on petroleum coke and biomass/coal co-gasification: Syngas production, reactivity characteristics, and synergy behavior. *Fuel*, 304, 121517. <https://doi.org/10.1016/j.fuel.2021.121517>
- [20] Khan, S., Elkadi, K., & Janajreh, I. (2023). Investigation of the co-gasification behavior of Kentucky coal and palm woody biomass. *Procedia Computer Science*, 224, 314-321. <https://doi.org/10.1016/j.procs.2023.09.042>
- [21] Zhou, T., Zhang, W., Shen, Y., Luo, S., & Ren, D. (2023). Progress in the change of ash melting behavior and slagging characteristics of co-gasification of biomass and coal: A review. *Journal of the Energy Institute*, 101414. <https://doi.org/10.1016/j.joei.2023.101414>
- [22] Lozynskiy, V. (2023). Critical review of methods for intensifying the gas generation process in the reaction channel during underground coal gasification (UCG). *Mining of Mineral Deposits*, 17(3), 67-85. <https://doi.org/10.33271/mining17.03.067>
- [23] Pivnyak, G., Dychkovskiy, R., Bobyliv, O., Cabana, E.C., & Smoliński, A. (2018). Mathematical and geomechanical model in physical and chemical processes of underground coal gasification. *Solid State Phenomena*, (277), 1-16. <https://doi.org/10.4028/www.scientific.net/ssp.277.1>
- [24] Saik, P., & Berdnyk, M. (2022). Mathematical model and methods for solving heat-transfer problem during underground coal gasification. *Mining of Mineral Deposits*, 16(2), 87-94. <https://doi.org/10.33271/mining16.02.087>
- [25] Lozynskiy, V., Saik, P., Petlovanyi, M., Sai, K., Malanchuk, Z., & Malanchuk, Y. (2018). Substantiation into mass and heat balance for underground coal gasification in faulting zones. *Inzynieria Mineralna*, 19(2), 289-300. <https://doi.org/10.29227/IM-2018-02-36>
- [26] Yang, M., Mousavi, S.M., Fatehi, H., & Bai, X.S. (2023). Numerical simulation of biomass gasification in fluidized bed gasifiers. *Fuel*, 337, 127104. <https://doi.org/10.1016/j.fuel.2022.127104>
- [27] Rehman, A.U., Unar, I.N., Abro, M., Qureshi, K., Almani, S., & Jatoti, A.S. (2023). Numerical simulations of gasification of low-grade coal and lignocellulosic biomasses in two-stage multi-opposite burner gasifier. *Processes*, 11(12), 3451. <https://doi.org/10.3390/pr11123451>
- [28] Zhang, H., Xiao, Y., Luo, G., Fang, C., Zou, R., Zhang, Y., Li, H., & Yao, H. (2024). Numerical simulation study on chemical ignition process of underground coal gasification. *Energy*, 298, 131350. <https://doi.org/10.1016/j.energy.2024.131350>
- [29] Tian, Z.F., Witt, P.J., Schwarz, M.P., & Yang, W. (2017). Numerical modeling of pulverised coal combustion. *Handbook of Multiphase Flow Science and Technology*, 1-35. https://doi.org/10.1007/978-981-4585-86-6_9-2
- [30] Kurose, R., Watanabe, H., & Makino, H. (2009). Numerical simulations of pulverized coal combustion. *KONA Powder and Particle Journal*, 27(0), 144-156. <https://doi.org/10.14356/kona.2009014>
- [31] Madejski, P. (2018). Coal combustion modelling in a frontal pulverized coal-fired boiler. *E3S Web of Conferences*, 46, 00010. <https://doi.org/10.1051/e3sconf/20184600010>
- [32] Prokhorov, D.A., & Piralishvili, Sh.A. (2020). Numerical simulation of pulverized coal combustion and comparison with in-furnace measurements. *Fundamental and Innovative Research for Improving Competitive Dignified Nation and Industrial Revolution 4.0*, 040008. <https://doi.org/10.1063/5.0000688>
- [33] Chen, G., Wang, H., Luo, K., & Fan, J. (2023). A DNS study of pulverized coal combustion in a hot turbulent environment: Effects of particle size, mass loading and preferential concentration. *Combustion and Flame*, 254, 112839. <https://doi.org/10.1016/j.combustflame.2023.112839>
- [34] Rabaçal, M., Costa, M., Rieth, M., & Kempf, A.M. (2020). Particle history from massively parallel large eddy simulations of pulverised coal combustion in a large-scale laboratory furnace. *Fuel*, 271, 117587. <https://doi.org/10.1016/j.fuel.2020.117587>
- [35] Saha, M., Chinnici, A., Dally, B.B., & Medwell, P.R. (2015). Numerical study of pulverized coal mild combustion in a self-recuperative furnace. *Energy & Fuels*, 29(11), 7650-7669. <https://doi.org/10.1021/acs.energyfuels.5b01644>
- [36] Mikulčić, H., von Berg, E., Vujanović, M., & Duić, N. (2014). Numerical study of co-firing pulverized coal and biomass inside a cement calciner. *Waste Management & Research: The Journal for a Sustainable Circular Economy*, 32(7), 661-669. <https://doi.org/10.1177/0734242x14538309>
- [37] Amritkar, A.R., Tafti, D., & Deb, S. (2012). Particle scale heat transfer analysis in rotary kiln. *Heat Transfer Summer Conference*, 9530962. <https://doi.org/10.1115/ht2012-58137>
- [38] Liang, Z., Peng, X., Huang, Z., Chen, J., Li, J., Yi, L., & Huang, B. (2023). Non-isothermal reduction kinetics of low-grade iron ore-coal mini-pellet in a low-temperature rotary kiln process. *Materials Today Communications*, 35, 105607. <https://doi.org/10.1016/j.mtcomm.2023.105607>
- [39] Chang, J., Ma, X., & Li, X. (2023). CPFD modeling of hydrodynamics, combustion and NO_x emissions in an industrial CFB boiler. *Particuology*, 81, 174-188. <https://doi.org/10.1016/j.partic.2022.12.019>
- [40] Sutardi, T., Wang, L., Paul, M.C., & Karimi, N. (2018). Numerical simulation approaches for modelling a single coal particle combustion and gasification. *Engineering Letters*, 26(2), 257-266.
- [41] Arasappan, Y. (2022). Mathematical simulation of pulverized coal combustion. *Acta Mechanica Slovaca*, 26(3), 64-69. <https://doi.org/10.21496/ams.2023.008>
- [42] Sakolaree, P., Rattanaphaibun, K., Sukhanonsawas, W., & Sukjai, Y. (2022). Numerical simulation and experimental validation of pulverized coal combustion by using CFD. *II International Scientific Forum on Computer and Energy Sciences (WFCEs-II 2021)*, 2656, 070009. <https://doi.org/10.1063/5.0099579>
- [43] Nicolai, H., Li, T., Geschwindner, C., di Mare, F., Hasse, C., Böhm, B., & Janicka, J. (2021). Numerical investigation of pulverized coal particle group combustion using tabulated chemistry. *Proceedings of the Combustion Institute*, 38(3), 4033-4041. <https://doi.org/10.1016/j.proci.2020.06.081>
- [44] Nematollahi, M., Sadeghi, S., Rasam, H., & Bidabadi, M. (2020). Analytical modelling of counter-flow non-premixed combustion of coal particles under non-adiabatic conditions taking into account trajectory of particles. *Energy*, 192, 116650. <https://doi.org/10.1016/j.energy.2019.116650>
- [45] Ma, P., Nicolai, H., Huang, Q., Debiagi, P., Berkel, L.L., Stagni, A., Yang, Y., & Li, S. (2024). Numerical investigation on pyrolysis and ignition of ammonia/coal blends during co-firing. *Combustion and Flame*, 261, 113268. <https://doi.org/10.1016/j.combustflame.2023.113268>
- [46] Zhang, Z., Chang, K., Si, M., Luo, Z., & Cheng, Q. (2024). Study on radiation characteristics of coal fired boiler changing with burnout rate. *Fuel*, 362, 130883. <https://doi.org/10.1016/j.fuel.2024.130883>
- [47] Ghose, P., Sahoo, T.K., & Sahu, A.K. (2022). Pulverized coal combustion computational modeling approach: A review. *Proceedings of the Institution of Mechanical Engineers, Part A: Journal of Power and Energy*, 237(4), 797-818. <https://doi.org/10.1177/09576509221132939>
- [48] Cai, R., Luo, K., Watanabe, H., Kurose, R., & Fan, J. (2020). Recent advances in high-fidelity simulations of pulverized coal combustion. *Advanced Powder Technology*, 31(7), 3062-3079. <https://doi.org/10.1016/j.apt.2020.05.001>
- [49] Miura, T. (2023). Simulation of pulverized coal combustion. *Proceeding of Energy and the Environment*, 1998, 33-38. <https://doi.org/10.1615/1-56700-127-0-50>
- [50] Chen, G., Wang, H., Luo, K., & Fan, J. (2023). A DNS study of pulverized coal combustion in a hot turbulent environment: Effects of particle size, mass loading and preferential concentration. *Combustion and Flame*, 254, 112839. <https://doi.org/10.1016/j.combustflame.2023.112839>
- [51] Zhang, P., Zhang, H., & Zhang, Y.F. (2024). Kinetic studies of ignition of coal char particle suspension in hot air. *Fuel*, 357, 129977. <https://doi.org/10.1016/j.fuel.2023.129977>
- [52] Luu, T.D., Shamooni, A., Kronenburg, A., Braig, D., Mich, J., Nguyen, B.D., Scholtissek, A., Hasse, C., Thäter, G., Carbone, M., Frohnäpfel, B., & Stein, O.T. (2024). Carrier-phase DNS of ignition and combustion of iron particles in a turbulent mixing layer. *Flow, Turbulence and Combustion*, 112(4), 1083-1103. <https://doi.org/10.1007/s10494-023-00526-y>
- [53] Barraza, C.L., Bula, A.J., & Palencia, A. (2012). Modeling and numerical solution of coal and natural gas co-combustion in a rotary kiln. *Combustion Science and Technology*, 184(1), 26-43. <https://doi.org/10.1080/00102202.2011.615769>
- [54] Macphee, J. E., Sellier, M., Jermy, M., & Tadulan, E. (2009). CFD modeling of pulverized coal combustion in a rotary lime kiln. *Seventh International Conference on CFD in the Minerals and Process Industries, CSIRO, Melbourne, Australia*, 9(11), 1-6.
- [55] Sahin, M., Ilbas, M., & Arslan, B. (2024). Entrainment effects on combustion and emission characteristics of turbulent non-premixed ammonia/air and methane/air swirl flames through a developed perforated burner. *The Canadian Journal of Chemical Engineering*, 102(3), 1066-1077. <https://doi.org/10.1002/cjce.25100>
- [56] Meller, D., Engelmann, L., Stein, O.T., & Kempf, A.M. (2023). Exhaust Gas Recirculation (EGR) analysis of a swirl-stabilized pulverized coal flame with focus on NO_x release using FPV-LES. *Fuel*, 343, 127939. <https://doi.org/10.1016/j.fuel.2023.127939>
- [57] Zhang, H., Lin, H., Zhou, X., Wang, X., Zheng, H., Liu, Y., & Tan, H. (2024). CFD modeling and industry application of a self-preheating pulverized coal burner of high coal concentration and enhanced combustion stability under ultra-low load. *Applied Thermal Engineering*, 253, 123831. <https://doi.org/10.1016/j.applthermaleng.2024.123831>

Чисельне моделювання спалювання вуглецевмісної сировини в каналі вугільного пласта

В. Лозинський

Мета. Визначення механізму процесу горіння вуглецевмісної сировини як пилувугільного палива в умовах циліндричної порожнини, сформованої у вугільному пласті, зосереджуючись на динаміці розповсюдження температурних полів, розподілі продуктів горіння та стабілізації процесу.

Методика. Дослідження виконувалося за допомогою CFD моделювання із застосуванням моделі горіння “спалювання без попереднього змішування” та турбулентної моделі k -епсилон. Вибір геометрії каналу довжиною 30 м та діаметром 1 м базується на попередніх розрахунках, які визначають її як оптимальну для досягнення ефективного процесу когазифікації. При моделюванні враховано теплообмін шляхом активації рівняння енергії для розрахунку теплопереносу, що дозволило врахувати генерацію тепла внаслідок хімічних реакцій горіння, а також його розповсюдження через конвекцію, теплопровідність і випромінювання.

Результати. Визначенні параметри стабілізації температурного поля на рівні 1540°C у зоні горіння через 24 години з поступовим зниженням температури до 520°C у нижній частині каналу. Реакція окислення відбувається на перших 6 метрах каналу із формуванням основного продукту горіння CO₂. Аналіз швидкості потоку показав високу турбулентність біля входу, що сприяє ефективному змішуванню палива з окиснювачем. Поступове зниження інтенсивності турбулентності забезпечує стабільний розподіл теплової енергії в нижній частині каналу.

Наукова новизна. Розроблено методологію для моделювання горіння пилувугільного палива в каналі вугільного пласта з обмеженою геометрією із урахуванням стадійного розвитку процесу (рання, середня, фінальна стадії). Виявлено закономірності стабілізації температурного поля та розподілу хімічних компонентів вздовж каналу.

Практична значимість. Результати дослідження слугують основою для оптимізації процесів підземного спалювання вугілля та когазифікації, спрямованих на підвищення ефективності роботи геореакторної системи.

Ключові слова: вугілля, чисельне моделювання, температурне поле, когазифікація, підземна газифікація вугілля

Publisher's note

All claims expressed in this manuscript are solely those of the authors and do not necessarily represent those of their affiliated organizations, or those of the publisher, the editors and the reviewers.